strain
An International Journal for Experimental Mechanics

Acoustic and Electromagnetic Emissions as Precursor Phenomena in Failure Processes

G. Lacidogna*, A. Carpinteri*, A. Manuello*, G. Durin†, A. Schiavi†, G. Niccolini† and A. Agosto†

*Department of Structural Engineering & Geotechnics, Politecnico di Torino, Corso Duca degli Abruzzi 24 – 10129 Torino, Italy
†National Research Institute of Metrology – INRiM, Strada delle Cacce 91 – 10135 Torino, Italy

ABSTRACT: In this work, we measured the electromagnetic field, given by the moving charges, during laboratory fracture experiments on specimens made of different heterogeneous materials. We investigated the mechanical behaviour of concrete and rocks samples loaded up to their failure by the analysis of acoustic emission (AE) and electromagnetic emission (EME). All specimens were tested in compression at a constant displacement rate and monitored by piezoelectric (PZT) transducers for AE data acquisition. Simultaneous investigation into magnetic activity was performed by a measuring device calibrated according to metrological requirements. In all the considered cases, the presence of AE signals has been always observed during the damage process, whereas it is very interesting to note that the magnetic signals were generally observed only in correspondence to sharp stress drops or the final collapse.

KEY WORDS: *acoustic emission, brittle failure, damage localisation, electromagnetic emission, fracture precursors, heterogeneous materials*

Introduction

A number of laboratory studies have revealed the existence of electromagnetic emission (EME) during fracture experiments carried out on a wide range of materials [1–8]. The EME during failure of materials is analogous to the anomalous radiation of geoelectromagnetic waves observed before major earthquakes [9–11], reinforcing the idea that the EME effect can be applied as a forecasting tool for earthquakes.

The present article focuses on EME and acoustic emission (AE) detected during laboratory compression tests on concrete and rock specimens. Investigation into EME signals caused by fracture can be used for rock specimens with low electrical conductivity. As AE and EME coincide when certain types of rocks fail, the influence of EM fields on the AE transducers has been previously evaluated to be minimised. Given a fracture event, the associated EME precedes the AE response, and the time delay corresponds to the difference in propagation velocities of sound and EM signals.

While the mechanism of AE is fully understood, being provided by transient elastic waves caused by stress redistribution following fracture propagation [12–17], the origin of EME from fracture is not completely clear, and different attempts have been made to explain it.

Models for EME

An explanation of the EME origin was related to dislocation phenomena [18, 19], which however are not able to explain EME from fracture in brittle materials where the motion of dislocations can be neglected [5]. The weakness of the 'dislocation movement hypothesis' was confirmed in some experiments, showing that the EME amplitude increased with the brittleness of the investigated materials [20]. In brittle materials, the fracture propagation occurs suddenly, and it is accompanied by abrupt stress drops in the stress–strain curve related to sudden loss in the specimen stiffness.

Another relevant attempt to explain the EME origin was made through the 'capacitor model', where EME is assumed to be caused by net charges of opposite sign appearing on the vibrating faces of opening cracks [3, 21]. This model is not widely accepted because an accelerated electric dipole created by charged opening cracks apparently does not explain EME from shearing cracks, which indeed are experimentally observed [5]. However, the general validity of this model can be maintained, because a certain separation between charged faces is guaranteed even in shear fractures.

Frid *et al.* [5] and Rabinovitch *et al.* [8] recently proposed a model of the EME origin where, following

doi: 10.1111/j.1475-1305.2010.00750.x

the rupture of bonds during the cracks growth, mechanical and electrical equilibrium are broken at the fracture surfaces with creation of ions moving collectively as a surface wave on both faces. Lines of positive ions on both newly created faces (which maintain their charge neutrality unlike the capacitor model) oscillate collectively around their equilibrium positions in opposite phase to the negative ones (see Figure 1). The resulting oscillating dipoles created on both faces of the propagating fracture act as the source of EME. The oscillations shown in Figure 1 are the atomic ones, which contributes to the general motion of the system and are the source of EM radiation. This happens in brittle or quasi-brittle materials, like rocks or concrete, when are mechanically excited. According to this model, the EME amplitude increases as long as a fracture propagates, because the rupture of new atomic bonds contributes to the EME. When fracture stops, the waves and the EME decay by relaxation.

Because larger fracture advancements produce larger stress drops, this model agrees with the results in compression tests on rock specimens obtained by Fukui *et al.* [7], which establish a relationship of proportionality between stress drop and intensity of related EME.

Experimental Set-up

Four specimens made of different brittle materials (Concrete, Syracuse Limestone, Carrara Marble and Green Luserna Granite) were examined in this study (Figure 2). They were subjected to uniaxial compression using a Baldwin servo-controlled hydraulic testing machine with a maximum capacity of 500 kN and load measurement accuracy of ±1.0%. This machine is equipped with control electronics which makes it possible to carry out tests in either load control or displacement control. Each test was performed in piston travel displacement control by setting constant piston velocity. The test specimens were arranged in contact with the press platens without any coupling materials, according to the testing modalities known as 'test by means of rigid platens with friction'.

As the authors explained in other studies [15, 22], in a compressive test with rigid platens, no coupling material between the external surfaces of the specimens and the platens is used. When the specimen surfaces are not perfectly smooth, shear stresses can take place in the inner part of the specimen during the loading phases. These stresses are capable of producing ultrasonic noises because of the friction between the specimen surfaces and the rigid platens, altering AE signal detection. A similar behaviour is observed by Zhang *et al.* [23] during compressive loading tests on granite specimens. On the other hand, a different situation would emerge for softer loading platens, equipped, for example, with a thin layer of Teflon in contact between the platen and the specimen. In this case, the platens would cause lateral deformation, giving rise to outward-directed shear forces at the interface. In both cases, the AE signals produced in the early stages of loading are not very frequent, of small amplitude, and precede the nucleation of the main cracks in compressed speci-

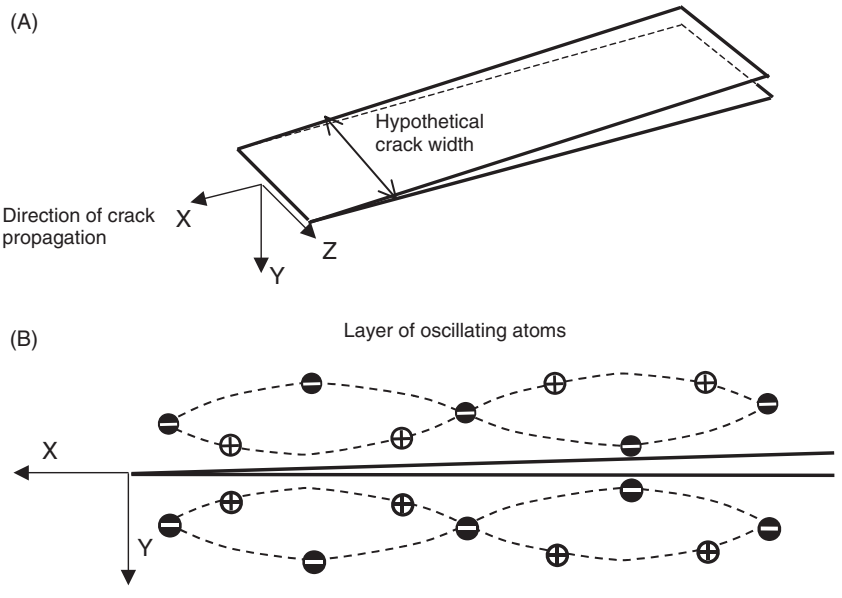

Figure 1: Picture of crack propagation and crack surfaces at a specific time. Crack surfaces are in the xz plane and the crack propagates in the *x* direction (A). Schematic representation at a specific time of surface waves propagating on the two newly formed crack surfaces. Layers of atoms move together generating surface vibrational waves on each face, where positive charges vibrate in opposite phase to the negative ones (B)

doi: 10.1111/j.1475-1305.2010.00750.x

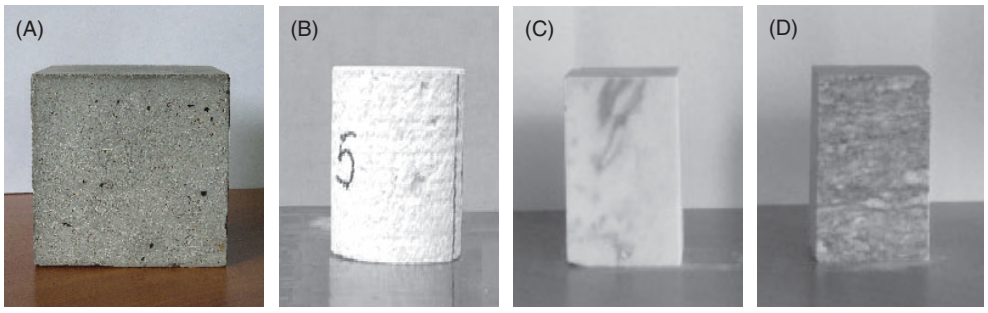

Figure 2: Views of test specimens: (A) Concrete, (B) Syracuse Limestone, (C) Carrara Marble and (D) Green Luserna Granite

Table 1: Materials, shapes, sizes of the tested specimens and piston velocities

Specimen	Material	Shape	Volume (cm^3)	Piston velocity ($m\ s^{-1}$)
P1	Concrete	Cubic	$10 \times 10 \times 10$	0.5×10^{-6}
P2	Syracuse Limestone	Cylindrical	$\pi \times 2.5^2 \times 10$	1.0×10^{-6}
P3	Carrara Marble	Prismatic	$6 \times 6 \times 10$	0.5×10^{-6}
P4	Green Luserna Granite	Prismatic	$6 \times 6 \times 10$	2.0×10^{-6}

mens. For this reason, they tend to be negligible after the first stage of damage, with respect to the main AE activity because of the damage accumulation [24].

The tested materials, shapes and sizes of the specimens, and the employed piston velocities are listed in Table 1. The selected range of the piston velocities, reported in the table, are in the authors' experience the most suitable values to evaluate AE and EME activity in quasi-brittle materials such as concrete and rocks [15, 22, 25, 26].

AE and EME Measurements

The AE emerging from the compressed specimens was detected by applying to the sample surface a piezoelectric (PZT) transducer, sensitive in the frequency range from 50 to 500 kHz for detection of high-frequency AE. In the test on specimen P1 (see Table 1) also a PZT accelerometric transducer, sensitive in the frequency range from 1 to 10 kHz, was used for detection of low-frequency AE (elastic emission, or ELE) [26]. As shown in [26], the terms AE and ELE -used to identify the ultrasonic waves coming from the material during the damage process- are useful to underline the difference in the AE propagation at high and low frequency. In the case of AE, the longitudinal and/or shear wave propagation is attributed to the oscillations of material particles around their equilibrium positions during microcrack growth, while the growth of large crack is accompanied by high-amplitude and long-wavelength elastic vibrations (ELE), which are able to deform the bulk of the solid and break its continuity.

The EM emission was detected using an isotropic probe calibrated according to metrological requirements at the National Research Institute of Metrology (Turin, Italy) for measuring the magnetic component of EM fields. The adopted device (Narda ELT-400 exposure level tester: Narda Safety Test Solutions An L-3 Communications Company Hauppauge, NY UNITED STATES) works in the frequency range between 10 and 400 kHz, the measurement range is between 1 nT and 80 mT, and the three-axial measurement system has a 100 cm^2 magnetic field sensor for each axis. This particular frequency range was chosen to avoid disturbances caused by radio waves that operate on medium frequencies of 300–3000 kHz, or other electronic devices that generally operate on frequencies above 3–30 MHz.

The device was placed 1 m away from the specimens. In Figure 3, the electromagnetic antenna and the AE acquisition system are shown.

Specific tests were conducted to assess the potential EM environmental noise, and what affecting the EM

Figure 3: Photograph of the compressive test on the Green Luserna Granite specimen. The electromagnetic antenna and the acoustic emission acquisition system are shown

doi: 10.1111/j.1475-1305.2010.00750.x

signals caused by the Baldwin test machine electronic control. In particular, the EM probe was used to detect the EM background noise for about five hours before the beginning of each compressive test. The background noise was estimated at about 40 nT in the frequency range 10 Hz–400 kHz. As regards the EM noise affecting the Baldwin machine electronic control, a characteristic signal of about 5 MHz was recognised.

Data acquisition of the EME signals was triggered when the magnetic field exceeded the threshold fixed at 0.2 μT after the preliminary measurements to filter out the magnetic noise in the laboratory. The recorded AE and EME signals were related to the time history of the load applied to the specimens.

Test Results

All specimens were tested in compression up to failure, showing a brittle response with a rapid decrease in load-carrying capacity when deformed beyond the peak load (Figures 4–7). Experimental evidence indicates the presence of AE and EME: an increasing AE activity is always detected as the load increases, while EME is only observed when abrupt stress drops occur. In the following sections, we focus on specimens P1 and P2 (Figures 4 and 5), representing two typical examples of catastrophic and quasi-brittle behaviours [27–29].

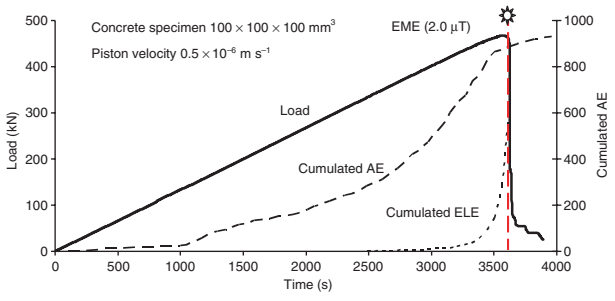

Figure 4: Load versus time curve of the Concrete specimen P1 (bold line). The dashed line and the dotted line represent the cumulated number of acoustic emission (high-frequency) and ELE (low-frequency), respectively. The star on the graph shows the moment of electromagnetic emission signal with a magnetic component of 2.0 μT

The Concrete specimen P1 exhibits a very steep softening branch (descending part of the stress–strain curve), which is referred to as 'snap-back' or catastrophic behaviour (Figure 4) [27–29]. On the other hand, the Syracuse Limestone, specimen P2, retains considerable strength beyond the peak load. Despite their different mechanical behaviours, specimens P1 and P2 both generate EME during sharp stress drops: P1 only at the peak load, whereas P2 even at the two intermediate stress drops occurred before the peak load. No further EME signals were detected in the post-peak region (Figure 5).

The Concrete specimen P1, subjected to AE, ELE and EME monitoring [25, 26], is characterised by a load versus time diagram almost linear up to failure. At 70% of the peak load, we observed a significant increase in the AE rate (the slope of the dashed line in Figure 4) and the appearance of ELE (the dotted line in Figure 4). At 90% of the peak load, the ELE rate increases dramatically, while the AE rate suddenly drops down. This evidence clearly indicates the transition from a microcracking-dominated damage process (revealed by the AE occurrence) to a process dominated by the propagation of a few large cracks and ELE.

Therefore, AE and ELE are both fracture precursors, while an EME signal (with magnetic component of 2 μT) was detected just in correspondence to the abrupt stress drop occurred at the specimen collapse (i.e. at the peak load).

The Syracuse Limestone specimen P2, subjected to AE and EME monitoring, is characterised by a more complex load versus time diagram because of

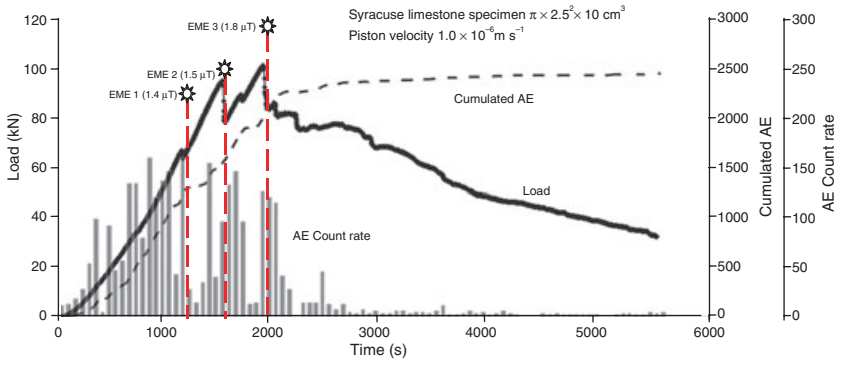

Figure 5: Load versus time curve of the Syracuse Limestone specimen P2 (bold line). The cumulated number of acoustic emission (AE) (dashed line) and the AE count rate obtained during the test are represented. The stars on the graph show the moments of electromagnetic emission signals with magnetic component comprised between 1.4 and 1.8 μT

doi: 10.1111/j.1475-1305.2010.00750.x

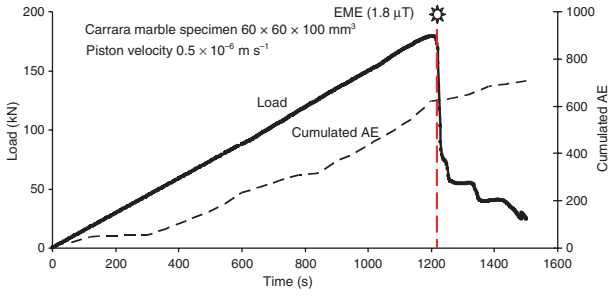

Figure 6: Load versus time curve of the Carrara Marble specimen P3 (bold line). The dashed line represents the cumulated number of acoustic emission. The star on the graph shows the moment of electromagnetic emission signal (magnetic component of 1.8 μT)

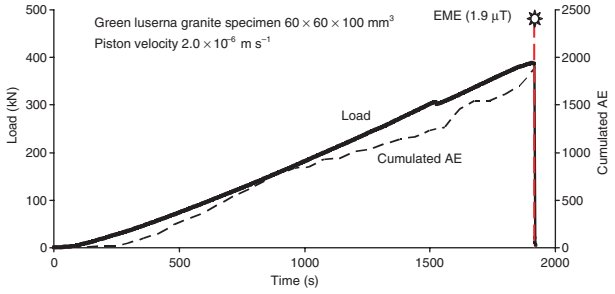

Figure 7: Load versus time curve of the Green Luserna Granite specimen P4 (bold line). The dashed line represents the cumulated number of acoustic emission. The star on the graph shows the moment of electromagnetic emission signal (magnetic component of 1.9 μT)

the heterogeneity of limestone. We observed three stress drops followed by as many drops in the AE rate, suggesting momentary relaxation after sudden crack advancements (Figure 5). This relaxation is clearly shown in Figure 5, where the AE count rate (numbers of AE signals per minute) is also reported. After the stress drops, AEs are very low during the reloading of the material until the stress exceeds the previous reached values (Kaiser effect) [12].

Even in this case, we detected three EM signals (with magnetic components ranging between 1.4 and 1.8 μT) in correspondence to each observed stress drop until the peak load is reached. The first stress drop occurred at 70% of the peak load, and the last one occurred at the peak load. It is worth noting that the EME intensity apparently does not depend, or depends weakly, as observed in [7], on the stress drop. In fact, similar magnetic components are associated with different stress drops. In particular, the first stress drop is clearly the smallest.

During the post-peak stage, that is softening branch in the load versus time diagram, no further EME signals were detected. In fact, at the peak load the fracture is completely formed, and the subsequent stages are characterised only by the opening of fracture surfaces. According to the model proposed by Frid *et al.* [5] and Rabinovitch *et al.* [8], this means that no newly broken atomic bonds can contribute to EME.

Similar results are shown in the cases of specimens P3 (Carrara marble) and P4 (green Luserna granite), reported in Figures 6 and 7. For these specimens, the EM signals with magnetic components of 1.8 μT (P3) and 1.9 μT (P4) are localised in correspondence to the peak load.

As shown in Figures 4–7 at the beginning of damage process, AE signals are emitted only at high frequencies, indicating microcrack initiation. Later on, at 70% of the peak load, we observed a significant increase in the AE rate, which damps as the peak load is approached. In fact, as observed during the monitoring of specimen P1, during the last phase of damage, an abrupt increase in AE signals at low frequencies (ELE) reveals that the final stage of damage process is dominated by the propagation of large cracks leading to the specimen failure. From these observations, therefore, emerges that the typical ultrasonic signal frequencies gradually decrease approaching to the critical stage of damage phenomenon [26]. This is also recently observed in [30], where it is reported that the average frequency of AE waveforms decreases as the damage accumulates in concrete and this parameter can be used for the characterisation of the failure process. Specific tests will be performed to detect ELE in materials such as Syracuse Limestone, Carrara Marble and Green Luserna Granite.

Summarising, the AE activity behaves as fracture precursor because it precedes EME events, which accompany stress drops and related discontinuous fracture advancements. The AE activity in the frequency range from 50 to 500 kHz indicates microcrack growth, while ELE appearance (from 1 to 10 kHz), as observed in specimen P1 (see Figure 4), suggests an increase in the density of microcracks and their coalescence into large cracks. According to the mentioned model [5, 7, 8], EME is associated with both micro and macrocrack growth, the latter revealed by abrupt stress drops. In the literature, similar experiments have been shown using electromagnetic antennas working in a frequency range from 10 kHz to 10 MHz [31]. Anyway, the adopted set-up for EME detection -threshold fixed at 0.2 μT, frequency range 10 Hz to 400 kHz- is not suitable for detection of microcracks, because the EME amplitudes associated with microcracks are lower than the fixed threshold, and the EME frequencies are beyond the observed frequency range.

doi: 10.1111/j.1475-1305.2010.00750.x

Arrival Time Estimation of AE and EME

An attempt to correlate AE and EM signals with the same fracture event was made, connecting the outputs of the PZT transducer and the magnetic tester to the same oscilloscope with sampling rate recording of 10 MSa s^{-1}. The problem of interest is to determine the location of a radiating source using the signals recorded from a number of sensors in the vicinity of the source. The source location can be calculated from a set of arrival time differences between pairs of recorded signals.

Taking into account the different propagation velocities v_{AE} and v_{EME}, a difference between arrival times of AE and EME signals is expected. The arrival time difference can be used to localise the radiating fracture (distant d from the AE transducer and d' from the magnetic tester):

$$\Delta t = \frac{d}{v_{AE}} - \frac{d'}{v_{EME}} \cong \frac{d}{v_{AE}}, \tag{1}$$

as $d'/v_{EME} << d/v_{AE}$.

The data acquired in a time window T can be represented by the time series $y_{EME}(t)$ and $y_{AE}(t)$ of the magnetic field measured by the tester and the output voltage of the AE transducer. The difference Δt of arrival information is obtained from the cross-correlation of the two received signals $y_{EME}(t)$ and $y_{AE}(t)$. The cross-correlation can be calculated using the time average [32]:

$$R(\tau) = (1/T)\int_0^T y_{AE}(t)y_{EME}(t-\tau)\,dt. \tag{2}$$

When the functions $y_{EME}(t-\tau)$ and $y_{AE}(t)$ match, the value of the integral $R(\tau)$ is maximised.

We applied the cross-correlation algorithm (2) to measure the time delays between AE and EME signals simultaneously acquired during the loading process on the specimens P1 and P2 (Figure 8A, B respectively). To compare these signals, only the module envelope is considered. In fact, the cross-correlation algorithm supports a visual 'peak picking' alignment approach, to improve the estimation of the arrival times. It is recommended in literature, instead of absolute arrival times, to evaluate the time delay between two signals with short time duration [33].

In the case of specimen P1, the EME signal detected at the peak load and the corresponding AE signal are represented in Figure 8A. The cross-correlation function $R(\tau)$ has a sharp peak at $\tau_0 = (0.7 \pm 0.1)$ μs, which estimates the time delay, $\Delta t = \tau_0$ between the EME and the AE signals. Specific measurements to determine the elastic wave velocity on the concrete specimen P1 were taken before the tests, obtaining an average measured velocity of about 4×10^3 m s^{-1}. Assuming that, even during the fracture damage propagation, the speed of sound in the concrete specimen is $v_{AE} \cong 4 \times 10^3$ m s^{-1}, Equation (1) estimates the distance between the radiating fracture

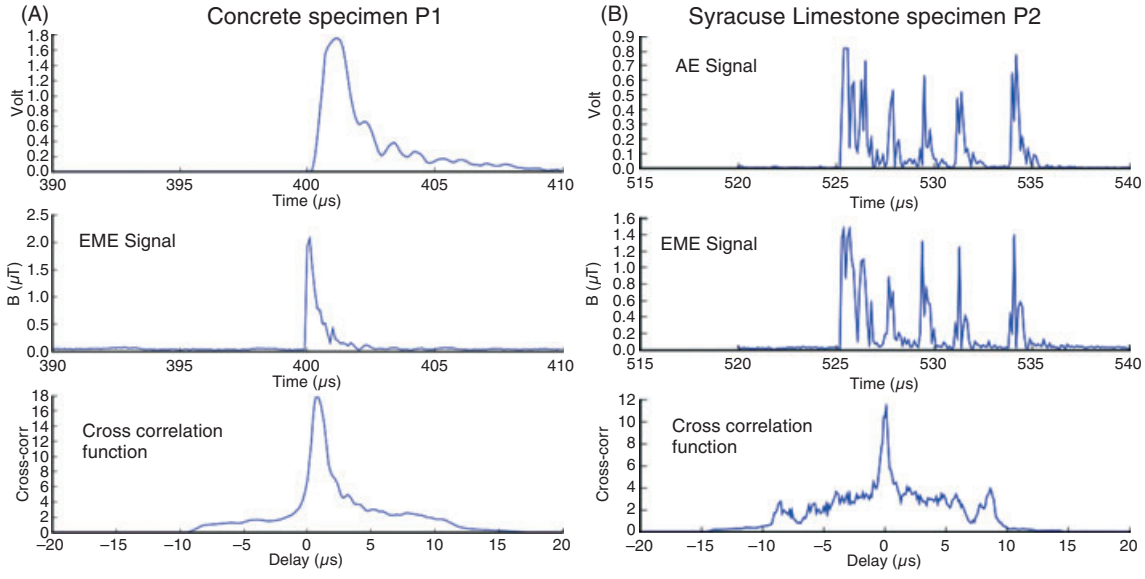

Figure 8: (A) Acoustic emission (AE) and electromagnetic emission (EME) (magnetic component of 2 μT) signals detected at failure of the Concrete specimen P1. (B) AE and EME (magnetic component of 1.5 μT) signals detected on the Syracuse Limestone specimen P2. (Upper): AE voltage signal. (Middle): magnetic component of the EME signal. (Lower): cross-correlation function where the peak estimates the time delay between the signals ($\tau_0 = 0.7$ μs for specimen P1 and $\tau_0 = 0.1$ μs for specimen P2)

doi: 10.1111/j.1475-1305.2010.00750.x

and the AE transducer position, given by $d \cong (2.8 \pm 0.4) \times 10^{-3}$ m.

Concerning specimen P2, we chose the $R(\tau)$ function relative to the second EME signal. The cross-correlation has a sharp peak at $\tau_0 = (0.1 \pm 0.1)$ μs (Figure 8B), implying that the radiating fracture was just at the specimen surface.

Moreover, it must be stressed that P1 e P2 are small size specimens, $10 \times 10 \times 10$ cm^3, and $\pi \times 2.5^2 \times 10$ cm^3 respectively (see Table 1). In this case, the time delays, $\tau_0 = (0.7 \pm 0.1)$ μs, or even $\tau_0 = (0.1 \pm 0.1)$ μs, are comparable to the measurement errors, because of the short travel path of the acoustic wave in the solid. In other words, the short time delay between AE and EM signal depends on the specimen size and on the closeness of the crack point to the specimen surface. Actually, considering real structures with characteristic size larger than 10 m, time delays of the order of 10–100 μs are expected.

Sensitivity of AE Transducers to EM Fields

To investigate simultaneously EME and AE during fracture experiments, it is necessary to set an appropriate threshold for the EME signals. This operation filters out the environmental EM fields. In our case, we set the threshold to 0.2 μT.

Furthermore, the AE transducers sensitivity to EM fields should be analysed. In fact, the AE signal originated from a fracture event might be the sum of the true AE wave and a voltage induced by the EME generated by the fracture itself. This is a relevant issue if we are interested in measuring time delays between AE and EME signals to perform crack localisation.

We evaluated the sensitivity of the two employed AE transducers to the EM disturbances. For this purpose, we exposed the AE transducers to sinusoidal magnetic fields with intensity (of 2 and 4 μT) close to the EME intensity recorded during fracture tests. The frequency of the applied magnetic field was 100 kHz, selected within the range (10 Hz–400 kHz) of the magnetic tester adopted for EME detection (see Figure 9).

The intensity of the applied magnetic fields was similar to that of EME accompanying fracture events. Therefore, we could compare the induced response of the transducers to the AE signals detected during fracture tests. The AE signals induced by the magnetic field were 2–3 orders of magnitude smaller than AE signals accompanying fracture events (compare Figures 8 and 9). Therefore, the strong AE signals detected in coincidence with EME during fracture tests should be really considered as genuine AE signals.

Conclusions

It is widely reported that changes in geoelectric potential and anomalous radiation of geoelectromagnetic waves, especially in low-frequency bands, occur before major earthquakes. At the laboratory scale, similar phenomena have also been observed on rock specimens under loading. In this case, crack growth is accompanied by AE ultrasonic waves and by redistribution of electric charges.

We investigated the mechanical behaviour of rocks and concrete samples loaded in compression up to their failure by the analysis of AE and EME signals. All specimens were tested in compression at constant displacement rate and monitored by PZT transducers

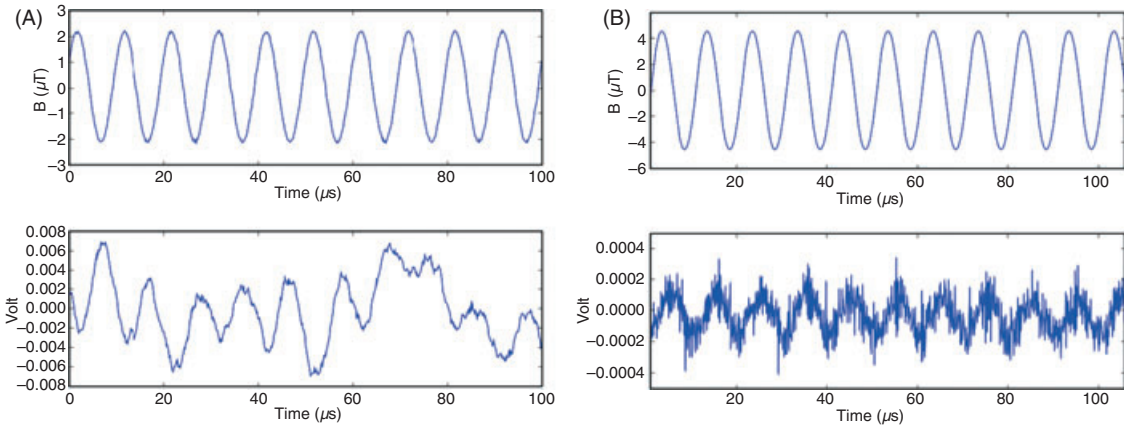

Figure 9: (A) Externally imposed 100 kHz magnetic (upper) and induced response of the accelerometric acoustic emission (AE) transducer employed during concrete fracture test (lower). (B) Externally imposed magnetic field (upper) and induced response of the HF AE transducer employed during Syracuse Limestone fracture test (lower). Under the same magnetic field intensity, the induced signals are 2–3 orders of magnitude smaller than AE signals caused by fracture (compare to Figure 8)

doi: 10.1111/j.1475-1305.2010.00750.x

for AE data acquisition. Simultaneous investigation into magnetic activity was performed by a measuring device calibrated according to metrological requirements. In all the considered cases, the presence of AE signals has been always observed during the damage process. Moreover, it is very interesting to note that the EME was generally observed only in correspondence to the sharp stress drops in the load versus time diagrams.

While the mechanism of AE is fully understood [12–17], we adopted the model proposed by Frid *et al.* [5] and Rabinovitch *et al.* [8] to explain the EME origin, according to which EME is generated by oscillating dipoles created by ions moving collectively as a surface wave on both faces of the crack. This model accounts correctly for the occurrence of the abrupt stress drops in load versus time diagrams because of sudden loss of specimen stiffness which accompanies discontinuous crack propagation [28, 29].

A study on the arrival time estimation of the AE and EME signals at the respective sensors is presented for an effective localisation of the radiating fractures in the materials. Further studies on the influence of magnetic fields to the AE transducers have been performed to assure a correct estimation of arrival time differences between AE and EME signals.

The experimental evidence presented in this article confirms the simultaneous investigation into AE and EME signals as collapse precursors in materials like rocks and concrete. From the presented studies turns out that EME detection may be used for damage location, using six EM sensors for 3D location of source cracks, likewise AE technique. However, the main advantage using EME in the monitoring of fracture is that the signal propagation is not affected by refraction and reflection phenomena as in the case of AE. Moreover, the antennas used for the acquisition of EME do not require to be applied on the external surface of the monitored specimen or structure as in the case of AE transducers.

Therefore, crack location by means of EM sensors would be easier to carry out also in the case of a civil structure like a bridge, a tunnel or a dam, but the presence of ferromagnetic materials can affect the EME results. Solving these problems needs further tests both in laboratory and on full size structures. Specific tests will be conducted to identify the relationships between the magnetic field and the size of the fracture and to evaluate the signal damping of EME in concrete and rocks.

Furthermore, the observed magnetic activity from laboratory experiments looks promising for effective applications also at the geophysical scale.

ACKNOWLEDGEMENTS

The financial support provided by the Regione Piemonte RE-FRESCOS Project, is gratefully acknowledged. Special thanks are due to Mr V. Di Vasto from the Politecnico di Torino for his collaboration in the execution of mechanical compressive tests. The authors are also grateful to Dr. Eng. Pavoni Belli of the National Research Institute of Metrology – INRIM for his valuable assistance in the AE signals elaboration process.

REFERENCES

1. Warwick, J. W., Stoker, C. and Meyer, T. R. (1982) Radio emission associated with rock fracture: possible application to the great Chilean earthquake of May 22, 1960. *J. Geophys. Res.* **87**, 2851–2859.
2. Ogawa, T., Oike, K. and Miura, T. (1985) Electromagnetic radiation from rocks. *J. Geophys. Res.* **90**, 6245–6249.
3. O'Keefe, S. G. and Thiel, D. V. (1995) A mechanism for the production of electromagnetic radiation during fracture of brittle materials. *Phys. Earth Plant. Inter.* **89**, 127–135.
4. Lolajicek, T. and Sikula, J. (1996) Acoustic emission and electromagnetic effects in rocks. In: *Progress in Acoustic Emission VIII. Proceedings of the 13th International Acoustic Emission Symposium*, 30 November, 1996. (Kishi, T., Mori, Y., Higo, H. and Enoki, M., Eds). Japanese Society for NDI, Nara, Japan: 311–314.
5. Frid, V., Rabinovitch, A. and Bahat, D. (2003) Fracture induced electromagnetic radiation. *J. Phys. D. Appl. Phys.* **36**, 1620–1628.
6. Hadjicontis, V., Mavromatou, C. and Nonos, D. (2004) Stress induced polarization currents and electromagnetic emission from rocks and ionic crystals, accompanying their deformations. *Nat. Hazards and Earth System Science* **4**, 633–639.
7. Fukui, K., Okubo, S. and Terashima, T. (2005) Electromagnetic radiation from rock during uniaxial compression testing: the effects of rock characteristics and test conditions. *Rock Mech. Rock Eng.* **38**, 411–423.
8. Rabinovitch, A., Frid, V. and Bahat, D. (2007) Surface oscillations. A possible source of fracture induced electromagnetic oscillations. *Tectonophysics* **431**, 15–21.
9. Gokhberg, M. B., Morgunov, V. A., Yoshino, T. and Tozawa, I. (1982) Experimental measurement of electromagnetic emissions possibly related to earthquakes in Japan. *J. Geophys. Res.* **87**, 7824–7828.
10. Nagao, T., Enomoto, Y., Fujinawa, Y. *et al.* (2002) Electromagnetic anomalies associated with 1995 Kobe earthquake. *J. Geodyn.* **33**, 401–411.
11. Karamanos, K., Dakopoulos, D., Aloupis, K. *et al.* (2006) Preseismic electromagnetic signals in terms of complexity. *Phys Rev E* **74**, 016104.
12. Kaiser, J. (1950) An investigation into the occurrence of noises in tensile tests, or a study of acoustic phenomena in tensile tests. Ph. D. dissertation, Munich (FRG), Technische Hochschule München.
13. Pollock, A. A. (1973) Acoustic emission-2: acoustic emission amplitudes. *Non-Destr. Test.* **6**, 264–269.

doi: 10.1111/j.1475-1305.2010.00750.x

14. Ohtsu, M. (1996) The history and development of acoustic emission in concrete engineering. *Mag Concrete Res* **48**, 321–330.
15. Carpinteri, A., Lacidogna, G. and Pugno, N. (2007) Structural damage diagnosis and life-time assessment by acoustic emission monitoring. *Eng. Fract. Mech.* **74**, 273–289.
16. Carpinteri, A., Lacidogna, G. and Manuello, A. (2007) Damage mechanisms interpreted by acoustic emission signal analysis. *Key Eng. Mater.* **347**, 577–582.
17. Carpinteri, A., Lacidogna, G., Niccolini, G. and Puzzi, S. (2008) Critical defect size distributions in concrete structures detected by the acoustic emission technique. *Meccanica* **43**, 349–363.
18. Misra, A. (1977) Theoretical study of the fracture-induced magnetic effect in ferromagnetic materials. *Phys Lett* **62A**, 234–236.
19. Misra, A. (1978) A physical model for the stress-induced electromagnetic effect in metals. *Appl Phys* **16**, 195–199.
20. Jagasivamani, V. and Iyer, K. J. L. (1988) Electromagnetic emission during the fracture of heat-treated spring steel. *Mater. Lett.* **6**, 418–422.
21. Miroshnichenko, M. and Kuksenko, V. (1980) Study of electromagnetic pulses in initiation of cracks in solid dielectrics. *Sov. Phys.-Solid State* **22**, 895–896.
22. Carpinteri, A., Lacidogna, G. and Manuello, A. (2009) The *b*-value analysis for the stability investigation of the ancient Athena Temple in Syracuse. *Strain* doi: 10.1111/j.1475-1305.2008.00602.x.
23. Zhang, A., Wagner, F. C., Stanchits, S., Dresen, G., Andresen, R. and Haidekker, M. A. (1998) Source analysis of acoustic emission in Aue granite cores under symmetric and asymmetric compressive load. *Geophys. J. Int.* **135**, 1113–1130.
24. Lockner, D. A., Byerlee, J. D., Kuksenko, V., Ponomarev, A. and Sidorin, A. (1991) Quasi static fault growth and shear fracture energy in granite. *Nature* **350**, 39–42.
25. Lacidogna, G., Manuello, A., Durin, G., Niccolini, G., Agosto, A. and Carpinteri, A. (2009). Acoustic and magnetic emissions as precursor phenomena in failure processes, Proc. of SEM Annual Conference & Exposition on Experimental and Applied Mechanics, Albuquerque, 1-4 June 2009, Paper No. 540.
26. Schiavi, A., Niccolini, G., Tarizzo, P., Lacidogna, G., Manuello, A. and Carpinteri, A. (2009) High and low frequency elastic wave propagation in brittle materials under compression, Proc. of SEM Annual Conference & Exposition on Experimental and Applied Mechanics, Albuquerque, 1-4 June 2009, Paper No. 539.
27. Hudson, J. A., Crouch, S. L. and Fairhurst, C. (1972) Soft, stiff and servo-controlled testing machines: a review with reference to rock failure. *Eng. Geol.* **6**, 155–189.
28. Carpinteri, A. (1989) Cusp catastrophe interpretation of fracture instability. *J. Mech. Phys. Solids* **37**, 567–582.
29. Carpinteri, A. (1990) A catastrophe theory approach to fracture mechanics. *Int. J. Fract.* **44**, 57–69.
30. Soulioti, D., Barkoula, N. M., Paipetis, A., Matikas, T. E., Shiotani, T. and Aggelis, D. G. (2009) Acoustic emission behavior of steel fibre reinforced concrete under bending. *Constr and Build Mater* **23**, 3532–3536.
31. Scott, D. F., Williams, T. J. and Knoll, S. J. (2004) Investigation of electromagnetic Emissions in a deep underground mine, Proc. of the 23rd International Conference on Ground Control in Mining, Morgantown, 3-5 August 2004, 125–132.
32. Bendat, J. S. and Piersol, A. G. (1980) *Engineering Applications of Correlation and Spectral Analysis*. John Wiley & Sons, New York.
33. Daku, B. L. F., Kosteniuk, P. and Pruggerc, A. F. (2001) Refining visually estimated arrival times of short duration signals. *Measurement* **30**, 297–305.

doi: 10.1111/j.1475-1305.2010.00750.x